Effects of load reduction on forces and moments on the runner blades of a Kaplan turbine model

IOP Conference Series:
Earth and
Environmental Science

PAPER • **OPEN ACCESS**

Effects of load reduction on forces and moments on the runner blades of a Kaplan turbine model

To cite this article: Martina Nobilo *et al* 2024 *IOP Conf. Ser.: Earth Environ. Sci.* **1411** 012001

IOP Conf. Series: Earth and Environmental Science **1411** (2024) 012001 doi:10.1088/1755-1315/1411/1/012001

Effects of load reduction on forces and moments on the runner blades of a Kaplan turbine model

Martina Nobilo[1], **Saeed Salehi**[1,2] **and Håkan Nilsson**[1]

[1] Chalmers University of Technology, Gothenburg, Sweden
[2] Chalmers Industriteknik, Gothenburg, Sweden

E-mail: martina.nobilo@chalmers.se

Abstract. Today's electric energy system includes more renewable sources than ever before, with a large increase in wind and solar power. The intermittency of wind and solar power brings certain challenges in maintaining the balance of the electric grid. Hydropower has shown great potential in solving the grid balancing problem. However, historically hydropower has had a completely different role, covering only the base load. The water turbines were designed to operate at the best efficiency point for most of their lifetime, and other kinds of operation may cause unpredictable shortening of the lifetime of the machines. Safe operation and planned maintenance are of great importance for both continuous energy distribution and human safety. In order to use the potential of hydropower to operate with highly variable loads, more comprehensive studies need to be made on the effects of transient operation of water turbines. An extensive series of studies have been made in recent years on the transient operation of Francis turbines and pump turbines. However, transient operations of Kaplan turbines require more in-depth studies. The present work analyses the flow-induced forces and resulting torques and bending moments on the U9-400 Kaplan turbine model runner blades during a load reduction sequence. New implementations in the OpenFOAM open-source CFD code have been developed to extract the forces, torques and bending moments on individual blades with respect to coordinate systems rotating with each individual blade.

1 Introduction

The rapid technological development in the last century lead to a higher electric power demand that required increased electricity production from conventional sources of energy. Consequentially, the emissions to the atmosphere have increased. This created the need to increase the share of renewable electricity production, which is continuously growing each year [1]. The main increase in renewable electric energy production the last decades is through wind and solar power. The inherent intermittency of these sources is causing an imbalance in the electric grid that needs to be taken care of. Hydropower can solve this problem, as a fast-responsive electricity-generating system that is renewable and flexible at the same time [2]. Historically, hydropower has been used as a base load in power generation and it was originally designed to operate at the best efficiency point (BEP) for most of its lifetime. To achieve flexibility in the system, hydropower needs to operate outside the design condition and during transients much more than anticipated in the design stage, and this causes a shortening of the lifetime of the machine. In order to understand the effects of the off-design and transient operation on the machine, and to ensure a safe operation with highly variable loads, a more detailed analysis of the machine needs to be done. Computational Fluid Dynamics (CFD) can

provide detailed information on the flow during transient operations of water turbines. In recent years, a number of studies have been done using CFD to report the appearing flow structures during the transient operations of Francis turbines [3, 4, 5, 6, 7, 8] and pump-turbines [9, 10, 11]. However, transient operations of Kaplan turbines have not been investigated enough. Regulation of Kaplan turbines is done by simultaneously changing the angles of both the guide vanes and the runner blades [12]. The runner blade angle about each individual blade axis can be changed while the blades are rotating with the runner. The runner blades are attached to the hub through a complex system of bearings and mechanical parts [13]. Those are affected by the flow-induced forces on the blades, and there is a need to predict the wear of those components and plan maintenance in order to avoid their fatigue [14] and failure of the blades [15]. Therefore it is important to investigate the flow-induced forces that originally act on the blades and cause stresses on them [16] but are also transferred to the mechanical parts of the hub [17, 18]. The extraction of all forces, torques and bending moments acting on the mechanical parts in the hub from a CFD simulation requires that the flow-induced forces acting on each individual blade is extracted in a coordinate system that is rotating with the blade, with an origin related to the position of interest for the bending moments.

The present paper employs CFD to investigate the flow-induced forces and resulting torques and bending moments on a runner blade of the U9-400 Kaplan turbine model during a load reduction sequence (in propeller mode). The results will later be extended with changes in runner blade angle and used for further analysis of the effects on the bearings and mechanical parts of the runner hub.

2 Geometry and operating conditions

The CFD simulation is performed on the U9-400 Kaplan turbine model shown in figure 1a. The computational domain includes the spiral casing, 18 stay vanes, 20 guide vanes, the runner with 6 blades, and the draft tube. The diameter of the runner is $D = 400\,\text{mm}$ and it rotates with a rotational speed of $\omega = 870\,\text{rpm}$. The turbine prototype, located in the hydropower plant Porjus in Sweden, generates 10 MW at high load with the diameter of the runner $D = 1550\,\text{mm}$.

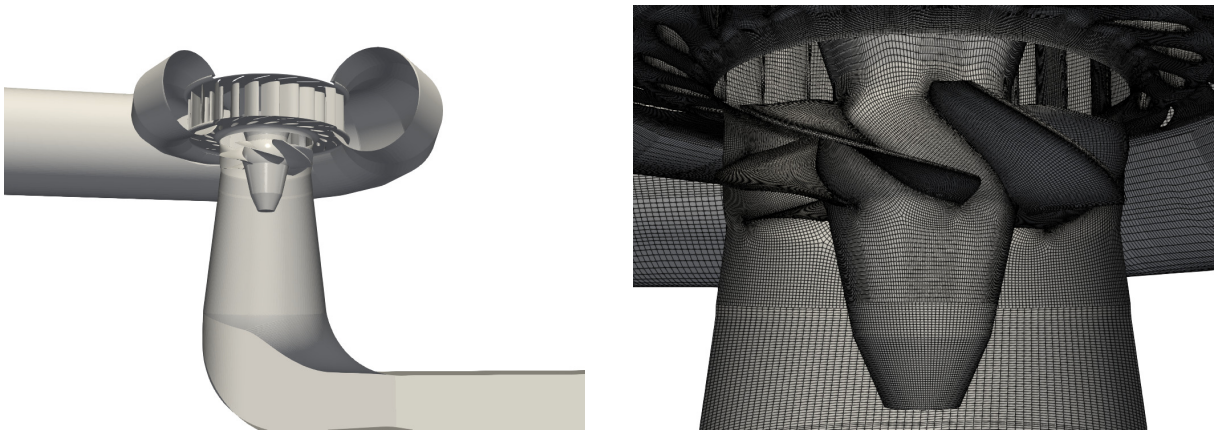

(a) Geometry (b) Computational mesh

Figure 1: The U9-400 Kaplan turbine model

The angles of both the guide vanes and the runner blades can be adjusted separately to control the operating condition in Kaplan turbines. However, the present work studies a load reduction sequence in propeller mode, i.e. with varying guide vane angle but fixed runner blade angle. The flow rate is controlled by closing the guide vanes by 6.5° during 4 seconds to achieve

the part load (PL) condition, where the initial opening angle of the guide vanes is 26.5° at the best efficiency point (BEP). This can be observed in figure 2, where the change of the guide vane angle and flow rate variation during the sequence are shown. The opening angle of the guide vanes can be read on the left vertical axis, while the flow rate is stated on the right vertical axis. The flow rate is given as an output of the solution, using the boundary conditions described in the following section. During this load reduction sequence, the flow rate is reduced from $Q_{\mathrm{BEP}} = 0.451\,\mathrm{m}^3/\mathrm{s}$ at BEP to $Q_{\mathrm{PL}} = 0.398\,\mathrm{m}^3/\mathrm{s}$ at PL, which is a reduction of around 12%.

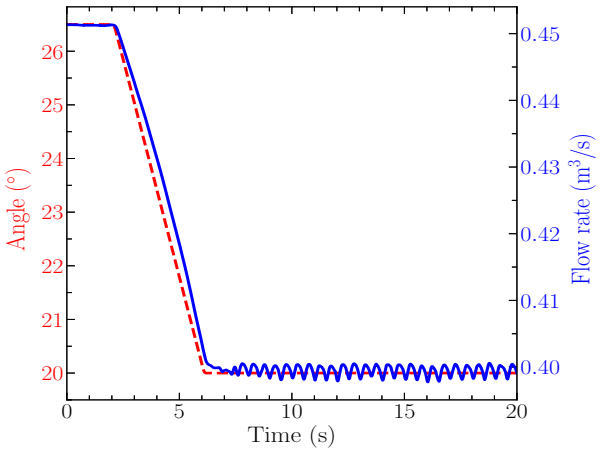

Figure 2: Flow rate response to change in guide vane angle

3 Numerical framework

The simulation was performed using OpenFOAM-v2112. The temporal derivatives are discretised with the implicit second-order backward scheme, while the second-order Linear-Upwind Stabilised Transport (LUST) scheme is used for the discretisation of the convective terms in the momentum equations. The pressure-velocity coupling is done using the PIMPLE algorithm, and the $k-\omega$ SST SAS model is adopted for the turbulence modelling. More details about the numerical framework of this case are available in our previous works [5].

The computational mesh is shown in figure 1b, with a total cell-count of 15×10^6. The inlet boundary is located at the beginning of the spiral casing, where a fixed total pressure of 84 940 Pa is utilised as a boundary condition. A static pressure boundary condition of $p = 0\,\mathrm{Pa}$ is prescribed at the outlet which is located at the end of the draft tube. The values correspond to those at steady BEP. These boundary conditions ensure that the flow rate is automatically adapted to the closing of the guide vanes, and that the flow rate variation is given as a result of the simulation. The change of angle of the guide vanes close to highly curved surfaces needs mesh morphing which is enabled by deploying the open-source semi-implicit slip mesh deformation algorithm developed by Salehi and Nilsson [19].

The flow-induced forces, torque and bending moments acting on one of the runner blades are obtained using a new implementation for the OpenFOAM open-source CFD code. It is developed to enable the calculation of the bending moments with respect to a local coordinate system that follows the blade rotation. To better explain the purpose of the implementation and the nomenclature used in this paper, a schematic illustration of the runner and one runner blade is presented in figure 3a. The analysis is made with respect to the location and orientation of the runner blade trunnion, shown in figure 3b. The interpretation of the coordinate axes is as follows:

- x and y are horizontal axes of the global coordinate system

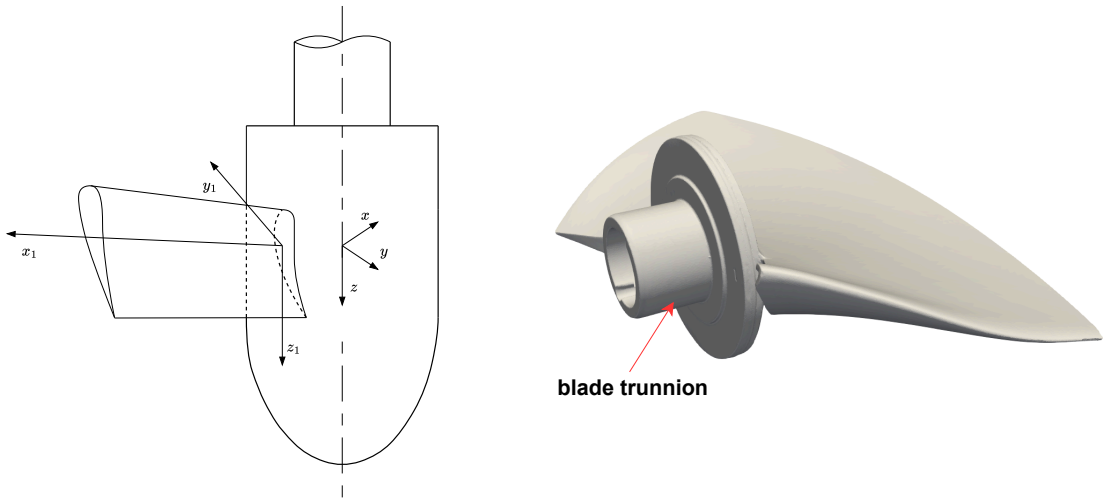

(a) Schematic illustration of a Kaplan runner with one blade and coordinate systems used.

(b) Runner blade scan, showing blade trunnion. Produced from blade scan in [20].

Figure 3: Geometry and coordinate system details

- z is the runner rotation axis in the global coordinate system
- x_1 is the runner blade trunnion rotation axis in the local coordinate system
- y_1 is the tangential direction of the blade in the local coordinate system
- z_1 is the axis in the local coordinate system that is parallel to the global z-axis

The global coordinate system is fixed in space with its origin at the axis of rotation of the runner. The local coordinate system has its origin at the blade trunnion axis, at an approximate position of the outer trunnion bearing. As the blade rotates, the local coordinate system needs to follow its rotation in order to keep the constant relations between the blade and the coordinate system axes. The developed utility enables recalculation of forces and moments on the blade with respect to the current position of the local coordinate system at every time-step.

4 Results and discussion

The results presented in this section show the time evolution of forces, torque and bending moments on one of the runner blades in a coordinate system that follows the runner blade rotation. To simplify the discussions, the following notation will be used, referring to the coordinate systems shown in figure 3a:

- F_{x_1} is the force acting in the axial direction of the runner blade trunnion
- F_{y_1} is the force acting in the tangential direction of the blade
- F_{z_1} is the force acting in the z_1 direction of the blade (same as axial direction of the runner)
- M_{x_1} is the torque around the trunnion axis x_1
- M_{y_1} is the bending moment around the y_1-axis
- M_{z_1} is the bending moment around the z_1-axis.

Figure 4 shows the time evolution of the force in the x_1 direction (F_{x_1}) and the torque about the x_1-axis (M_{x_1}) on one of the runner blades. The first two seconds show the BEP condition, in accordance with the operating sequence presented in figure 2. The force oscillations observed

during BEP will be analyzed in-depth in a later paragraph. With the start of the closing of the guide vanes at $t = 2\,\mathrm{s}$, the load reduction sequence begins and lasts for 4 s. During that sequence, the absolute mean value of both force and torque is decreasing, which is visible in figure 4. The changes in the amplitudes of the oscillations of force and torque during the load reduction sequence ($2\,\mathrm{s} \leq t \leq 6\,\mathrm{s}$) are shown in figure 5. These are obtained by subtracting the instantaneous mean value from the transient data. It can be observed that the amplitudes of both the force in the x_1 direction and the torque about the x_1 axis are decreasing during the transient part of the sequence. It shows that the closing of the guide vanes causes both a decrease of the absolute mean value and a decrease of the amplitude of the oscillations. At $t = 6\,\mathrm{s}$, the closing of the guide vanes stops and it can be seen in figure 4 that there is a short period of low-amplitude oscillations which is due to a delayed reaction of the system to the final position of the guide vanes. At around $t = 7.5\,\mathrm{s}$, high-amplitude low-frequency oscillations start to occur due to the formation of the rotating vortex rope (RVR) at the PL condition. These oscillations form a reoccurring pattern after $t = 11\,\mathrm{s}$, which suggests that the RVR is fully formed and a quasi-stationary PL condition is achieved until the end of the simulation. Only a short part of the BEP condition is shown in this paper, and the long simulation to establish the fully developed condition is excluded. The developed BEP condition is used as a starting point for the load reduction sequence. The PL condition is extended to get a fully developed PL condition for the analysis. The force oscillations observed during BEP and PL conditions are analysed in the following paragraphs.

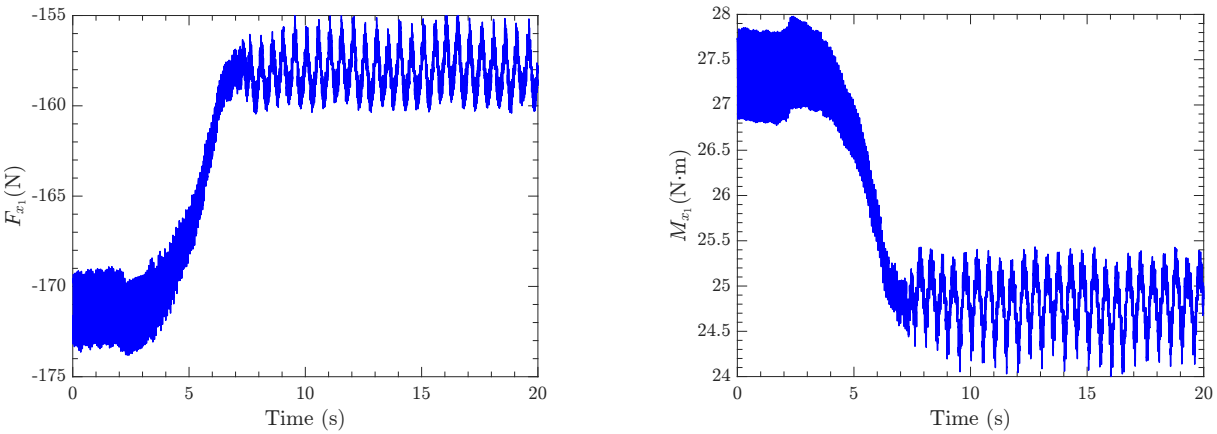

(a) Force in x_1-direction

(b) Torque about x_1-axis

Figure 4: Force and torque related to blade trunnion axial direction

Figure 6 shows the time evolution of the force in the x_1 direction (F_{x_1}) during the first 0.5 s of the BEP condition, and the accompanying fast fourier transform (FFT) of frequencies of the force. The frequency of the oscillations can be explained by observing the peaks in figure 6b. The frequencies at the horizontal axis are normalised with the rotational frequency of the runner, while the vertical axis shows the amplitude of the oscillation of the force. The highest peak is seen at $f/f_n = 1$, where the force frequency is matching the rotational frequency of the runner (14.5 rps). This matches the number of large oscillations in figure 6a, showing approximately seven ($\sim 14.5/2$) oscillations in 0.5 s. The exact cause of these oscillations needs to be further investigated, but it is related to a variation in the flow over a full runner rotation. Figure 6b also shows the harmonics of $f/f_n = 1$, but in particular an increased amplitude at $f/f_n = 20$. This corresponds to the rotor-stator interaction (RSI) between the runner blade and the 20 guide vanes. These oscillations can be seen in figure 6a as high-frequency oscillations on top of the runner frequency oscillations.

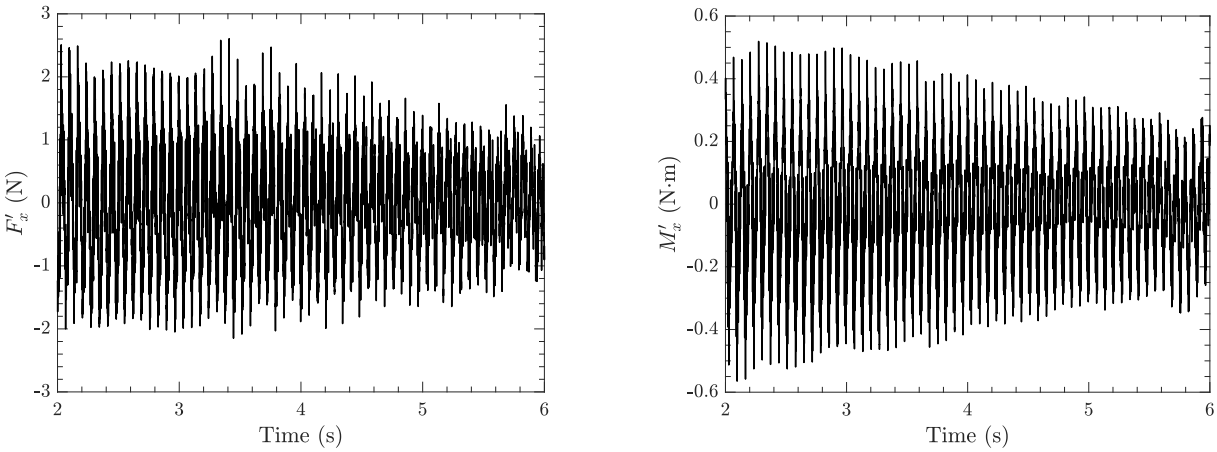

(a) Force in x_1-direction (b) Torque about x_1-axis

Figure 5: Amplitudes of force and torque oscillations during the closing of the GV

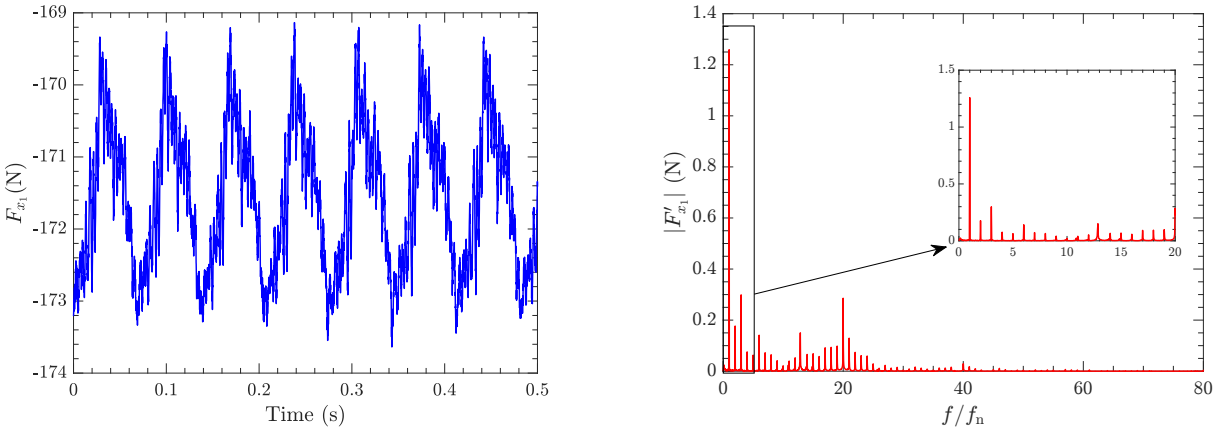

(a) Force in x_1 direction (b) FFT of force in x_1 direction

Figure 6: Force oscillations at BEP part of the sequence

Figure 7 shows the force in the x_1 direction (F_{x_1}) and the accompanying FFT during the quasi-stationary PL part of the sequence from $t = 11\,\text{s}$ to $t = 12\,\text{s}$. In figure 7a, the low-frequency high-amplitude oscillations repeating every 0.5 s are visible. The frequency of those oscillations can be observed in figure 7b as the frequency with the highest peak which occurs at at $f/f_n = 0.138$. This frequency matches a visually observed rotational frequency of the RVR. Figure 7b also shows increased amplitude at $f/f_n = 1$ and its harmonics, which was observed at BEP in figure 6b and related to a variation in the flow over a full runner rotation. The peak at $f/f_n = 1$ had by far the highest amplitude at BEP in figure 6b, while at PL its amplitude is not as distinct from others. The excitation at $f/f_n = 20$ in figure 7b corresponds to the frequency of the RSI between the runner blade and the 20 guide vanes, and can be recognized as high-frequency oscillations with the smallest amplitude in figure 7a. These oscillations were also observed in BEP condition in figure 6a, but with a higher amplitude in comparison to PL. This shows that the influence of the RSI is reduced at PL condition.

Figure 8 shows the time evolution of the forces in the other two directions (F_{y_1} and F_{z_1}) on the same runner blade. The magnitude of the force in the y_1 direction is double of that in the x_1 direction, and it is almost six times larger in the z_1 direction. The PL oscillation amplitude is

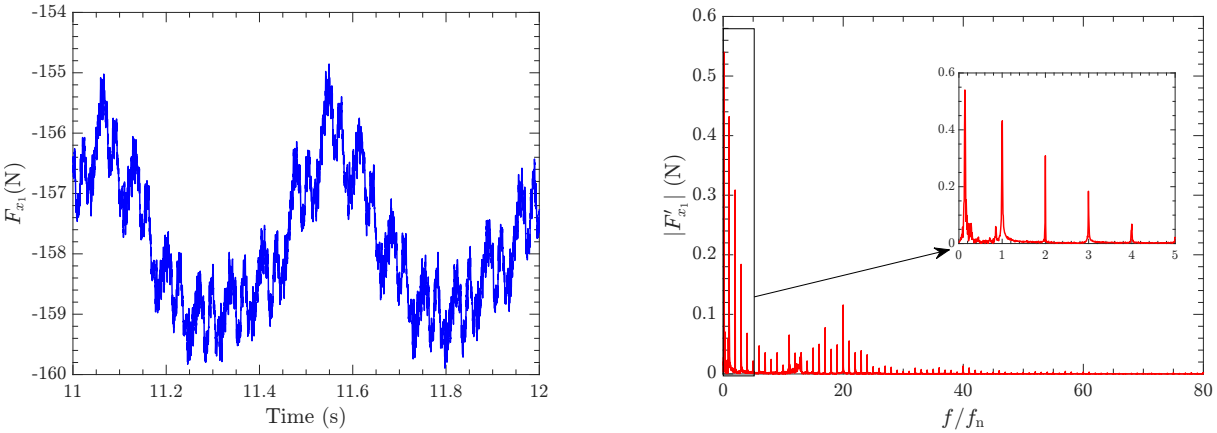

(a) Force in x_1 direction (b) FFT of force in x_1 direction

Figure 7: Force oscillations at PL part of the sequence

higher compared to the BEP amplitude for the F_{y_1} and F_{z_1} forces than for the F_{x_1} force. To give the reason behind this, it is necessary to analyse the FFTs of the forces. The individual FFTs of forces in y_1 and z_1 direction during PL condition can be observed in figure 9. The larger the difference in height of the peaks in the FFT, the higher the difference between the amplitudes of forces oscillations. It can be noticed that the peak at the RVR frequency at $f/f_n = 0.138$ in both figure 9a and figure 9b is more than two times higher than that at the rotational frequency of the runner ($f/f_n = 1$). The peak at the same frequency in figure 7b is only around 20% higher than the one at runner's frequency. This shows that the RVR causes higher amplitudes of force oscillations at the PL condition in the y_1 and z_1 directions in comparison to the the x_1 direction.

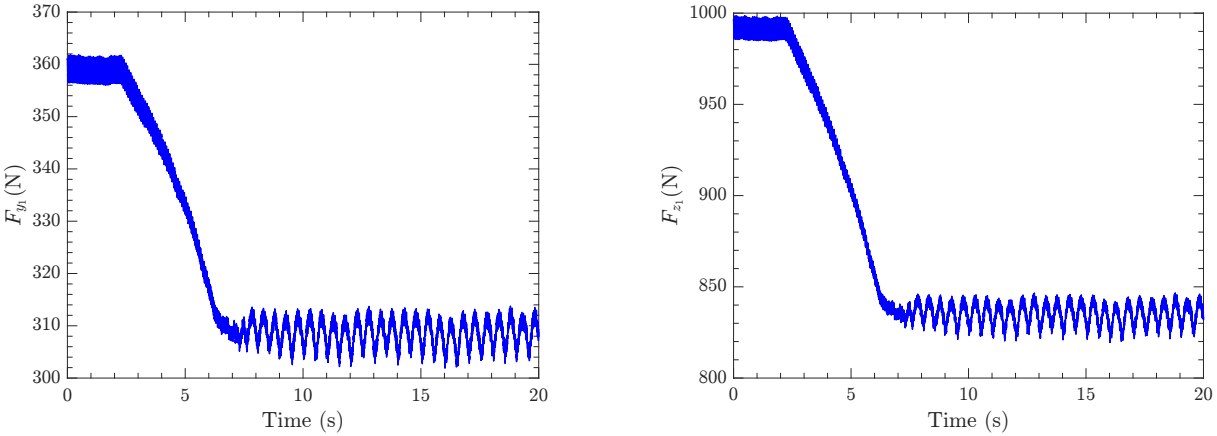

(a) Force in y_1-direction (b) Force in z_1-direction

Figure 8: Forces on the runner blade

Figure 10 shows the time evolution of the y_1 and z_1 bending moments (M_{y_1} and M_{z_1}) at a location corresponding to the runner blade trunnion outer bearing. It can be observed that the magnitude of the bending moment around the y_1-axis is twice as large as the magnitude of the bending moment around the z_1-axis. This is a direct consequence of the higher force magnitude in the z_1 direction, which causes the majority of the bending moment around the y_1-axis. This

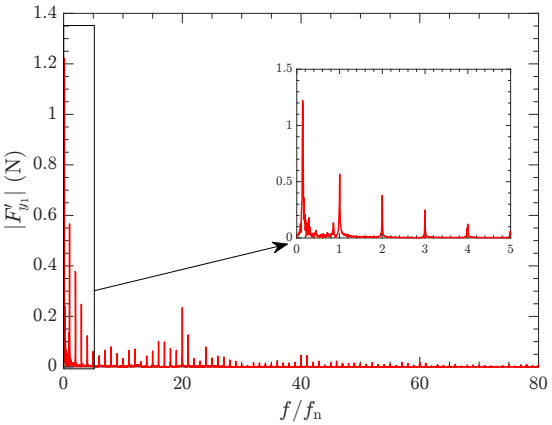

(a) FFT of force in y_1 direction

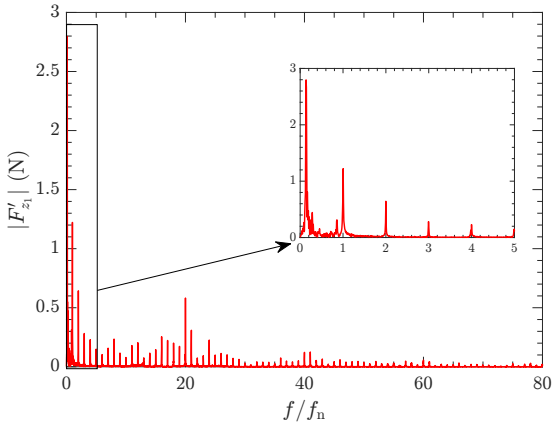

(b) FFT of force in z_1 direction

Figure 9: Force frequencies at PL part of the sequence

is also the reason why the time evolution of the bending moment around the y_1-axis has a very similar shape as the negative time evolution of the force in the z_1 direction. The bending moment around the z_1-axis is mainly caused by the force in the y_1 direction, and the shape of the time evolution of the bending moment around the z_1-axis is therefore almost identical to the time evolution of the force in the y_1 direction. Both bending moments show high-frequency oscillations at BEP as a consequence of the rotor-stator interaction, and also (additionally) low-frequency high-amplitude oscillations at PL due to the RVR. For the calculation of the bending moments around the y_1-axis (in figure 10a) and z_1 axis (in figure 10b) the implementation explained in section 3 is of great importance. It enables to extract the forces in the local coordinate system that matches the current position of the blade. It also enables calculation of position vectors of the runner blade mesh faces needed for the moment calculation in relation to that coordinate system. Without this implementation the extraction of the presented bending moments on the runner blade trunnion would not be possible.

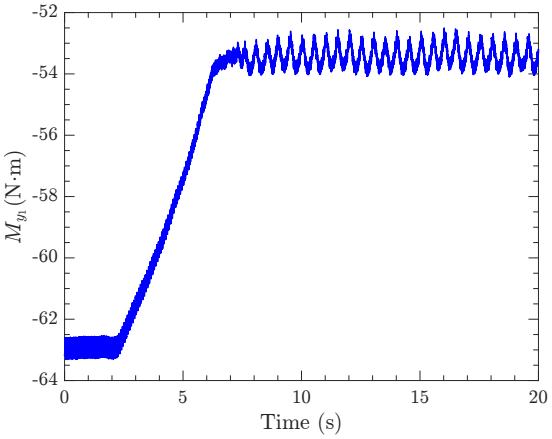

(a) Bending moment around y_1-axis

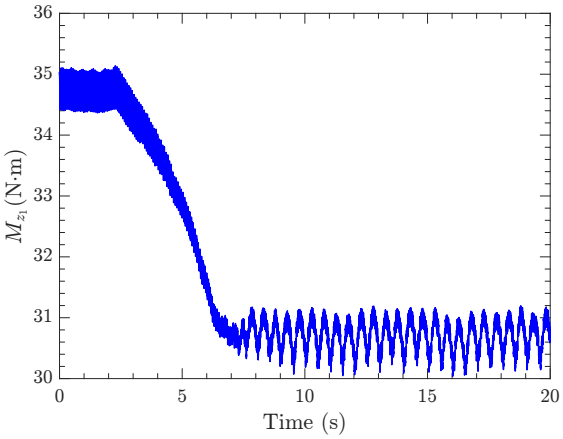

(b) Bending moment around z_1-axis

Figure 10: Bending moments at the runner blade trunnion outer bearing

5 Conclusion

This paper gives a detailed analysis of the time evolution of the forces, bending moments and torque acting on the trunnion of a Kaplan model turbine runner blade during a load reduction sequence from BEP to PL. The turbine was operated in propeller mode, meaning that the load reduction sequence was performed by closing the guide vanes while the runner blade angle remained fixed. The results were obtained using the OpenFOAM-v2112 open-source CFD code with a new addition for extracting the required data. Using both time evolution of forces and FFT of the signals, the origins of the forces oscillations were established. It was shown that oscillations of forces at BEP come from rotor-stator interactions. The high-frequency low-amplitude oscillations match the frequency of a runner blade interacting with the guide vanes. They are superimposed on high-amplitude oscillations that are matching the rotational frequency of the runner. The low-frequency high-amplitude oscillations visible at PL match a visually observed rotational frequency of the RVR. The low-amplitude high-frequency oscillations due to the rotor-stator interactions are superimposed on them. With further FFT analysis of the forces at PL condition it was shown that the RVR causes higher amplitudes of force oscillations in the y_1 and z_1 directions in comparison to the force in the x_1 direction. Extracted torque and bending moments were also presented and discussed in relation to the forces from which they were calculated. It was shown that the bending moment around the y_1 axis has the highest magnitude among the moments. This comes from the fact that the force in the z_1 direction has the highest magnitude, which causes the majority of the bending moment around the y_1-axis.

Acknowledgments

The research presented was carried out as a part of the "Swedish Centre for Sustainable Hydropower - SVC". SVC has been established by the Swedish Energy Agency, Energiforsk and Svenska kraftnät together with Luleå University of Technology, Uppsala University, KTH Royal Institute of Technology, Chalmers University of Technology, Karlstad University, Umeå University and Lund University.

The computations were enabled by resources provided by the National Academic Infrastructure for Supercomputing in Sweden (NAISS) at NSC and C3SE partially funded by the Swedish Research Council through grant agreement no. 2022-06725.

References

[1] REN21 2024 Renewables 2024 global status report collection
[2] Hell J 2017 *J. Phys.: Conf. Ser.* **813** p 012007
[3] Mössinger P, Jester-Zürker R and Jung A 2017 *J. Phys.: Conf. Ser.* **782** p 012001
[4] Salehi S, Nilsson H, Lillberg E and Edh N 2021 *IOP Conf. Ser.: Earth and Environmental Science* **774** p 012060
[5] Salehi S, Nilsson H, Lillberg E and Edh N 2021 *Renewable Energy* **179** pp 2322–2347 ISSN 0960-1481
[6] Salehi S and Nilsson H 2021 *OpenFOAM® Journal* **1** pp 47–61 ISSN 2753-8168
[7] Salehi S and Nilsson H 2022 *Renewable Energy* **188** pp 1166–1183 ISSN 0960-1481
[8] Salehi S and Nilsson H 2022 *Renewable Energy* **193** pp 57–75 ISSN 0960-1481
[9] Li Z, Bi H, Karney B, Wang Z and Yao Z 2017 *Journal of Hydraulic Research* **55** pp 520–537 ISSN 1814-2079
[10] Fahlbeck J, Nilsson H, Salehi S, Zangeneh M and Joseph M 2021 *IOP Conf. Ser.: Earth and Environmental Science* **774** p 012066
[11] Fahlbeck J, Nilsson H and Salehi S 2021 *Energies* **14** p 3593 ISSN 1996-1073
[12] Dixon S and Hall C 2010 Chapter 9 - Hydraulic Turbines *Fluid Mechanics and Thermodynamics of Turbomachinery (Sixth Edition)* ed Dixon S and Hall C (Boston: Butterworth-Heinemann) pp 303–355 ISBN 978-1-85617-793-1
[13] Barbosa R d S and Silva F d A 2013 *Proc. of the 22nd Int. Congress of Mechanical Engineering* pp 897–906
[14] Luo Y, Wang Z, Zeng J and Lin J 2010 *Engineering Failure Analysis* **17** pp 192–199 ISSN 1350-6307
[15] Zhang M, Valentín D, Valero C, Egusquiza M and Egusquiza E 2019 *Engineering Failure Analysis* **97** pp 690–700 ISSN 1350-6307
[16] Zhou L, Wang Z, Xiao R and Luo Y 2007 *Engineering computations* **24** pp 753–762 ISSN 0264-4401

[17] Cojocaru V, Miclosina C O, Campian C V, Frunzaverde D and Nedelcu D 2022 *IOP Conf. Ser.: Materials Science and Engineering* **1262** p 012046
[18] Luo Y, Yang G, Cao J, Yang J, Chen J, Zhao H and Wang Z 2023 *Journal of Energy Storage* **72** p 108269 ISSN 2352-1538
[19] Salehi S and Nilsson H 2023 *Computer Physics Communications* **287** p 108703 ISSN 1879-2944
[20] Amiri K, Mulu B, Raisee M and Cervantes M J 2017 *Journal of Applied Fluid Mechanics* **10** pp 1045–1059 ISSN 1735-3645